Control and Planning of 3D Dynamic Walking with Asymptotically Stable Gait Primitives

Robert D. Gregg*, Adam K. Tilton, Salvatore Candido, Timothy Bretl, and Mark W. Spong

***Abstract*—In this paper we present a hierarchical control framework that enables motion planning for three-dimensional bipedal dynamic walkers in the same way that planning is already possible for quasi-static walkers. This framework is based on the construction of *asymptotically stable gait primitives* for a class of hybrid dynamical systems with impacts. Each primitive corresponds to an asymptotically stable hybrid limit cycle that admits rules for sequential composition with other primitives, reducing a high-dimensional feedback motion planning problem into a low-dimensional discrete tree search. As an example, we construct asymptotically stable gait primitives for a 3D compass-gait biped using geometric reduction-based control, where in this case each primitive corresponds to walking along an arc of constant curvature for a fixed number of steps. We apply a discrete search algorithm to plan a sequence of these primitives taking the biped stably from start to goal in three-dimensional workspaces with obstacles.**

I. Introduction

The energetic efficiency of human bipedal locomotion is due primarily to its reliance on *dynamic walking*. During each step cycle, the body's center of mass engages in a controlled fall along a pendular arc until foot-ground impact redirects this motion into the next step cycle. Evidence suggests that, using this type of locomotion, human bipeds are more energetically efficient than quadrupeds at low speeds [30].

Most humanoid robots to date, such as HRP-2 [25] and Honda ASIMO [24], do not take advantage of dynamic walking. Instead, their motion is constrained by a "quasi-static" equilibrium condition. These bipeds prevent foot-ground rotation (i.e., falling) by ensuring there is zero net moment at the center of pressure (COP), the point on the support polygon/footprint where the resultant ground reaction force acts [43]. When strictly within the support polygon, the COP is equal to the *zero moment point* (ZMP) satisfying

$$M + R \times F \;=\; 0, \tag{1}$$

where R is the vector from the COP to the ankle, at which the body contributes linear force vector F and moment vector M [43]. When the ZMP exits the support polygon, the biped rotates about a new passive degree-of-freedom (DOF) at the COP on the boundary of the support polygon. This falling scenario is avoided by ZMP trajectory planners, whereas dynamic gaits substantially involve such pendular falling states.

Both forms of walking are mathematically represented by joint trajectories that evolve according to continuous and discrete dynamics in a *hybrid system*. This produces periodic orbits in system state called *hybrid limit cycles*. A *quasi-static* walking gait is then a hybrid limit cycle satisfying (1), and a *dynamic* walking gait is a hybrid limit cycle in which condition (1) is violated for some portion of the cycle.

Quasi-static gaits typically require large actuators to track constrained joint trajectories while actively supporting the body weight with flexed knees during the entire step cycle [28]. This results in shuffling motion that is up to an order of magnitude less efficient than dynamic walking in terms of energetic cost of transport [10]. The ZMP condition nonetheless provides a simple guarantee that the supporting foot does not rotate and the robot does not fall [43], even though the hybrid limit cycle may not be stable [44, Section 10.8]. For this reason, quasi-static motion planning and control strategies have so far dominated humanoid robotic walking.

Our goal in this paper is to enable motion planning for dynamic walkers in the same way that planning is already possible for quasi-static walkers. We will do so by constructing a set of dynamic "motion primitives" with safety guarantees that are amenable to established planning methods based on quasi-static motion primitives.

A. Quasi-Static Locomotion Planning

Motion primitives prescribe a library of common actions such as walking and climbing, reducing the high-dimensional kinodynamic planning problem to a discrete sequence of these pre-computed motions. For example, a set of quasi-static motion primitives was used in [22] to bias the sampling of configurations between planned sequences of discrete foot placements. Full-body posture and locomotion planning was enabled in [26], [27] by initially computing a large set of statically-stable configurations. Paths between goal configurations were then found by randomly growing a tree of nodes that connect only if a collision-free path exists satisfying (1).

The hierarchical planner in [46] modeled a 3D robot as a planar bounding box on the walking surface, restricting the search for walking paths to configuration space $\mathrm{SE}(2)$ – x, y position and orientation. Collision-free configurations were locally connected by Dubins curves (circular arcs with tangential line segments) to form quasi-static walking paths.

We will embrace a similar reduction in the path planning problem for dynamic walking through 3D space. Instead of using motion primitives that track quasi-static joint trajectories, we will build control systems yielding stable walking gaits.

R. D. Gregg is with the Department of Mechanical Engineering and the Rehabilitation Institute of Chicago, Northwestern University, Chicago, IL 60611 rgregg@northwestern.edu *Corresponding author.

S. Candido is with the Department of Electrical and Computer Engineering, A. K. Tilton is with the Department of Mechanical Science and Engineering, and T. Bretl is with the Department of Aerospace Engineering, University of Illinois at Urbana-Champaign, Urbana, IL 61801 {candido,atilton2,tbretl}@illinois.edu

M. W. Spong is with the Department of Electrical Engineering, University of Texas at Dallas, Richardson, TX 75080 mspong@utdallas.edu

This research was partially supported by NSF Grants CMMI-0856368, CMS-0510119, and NSF-0931871.

B. Dynamic Locomotion Planning

Dynamic walkers embrace ballistic momentum and gravitational potential energy for speed and efficiency, but these robots currently lack the same functionality as quasi-static humanoids, e.g., some require downhill slopes for gravity-powered walking, are constrained to the sagittal plane-of-motion, lack directional control authority, and/or lack redundant joints for manipulation. Hybrid nonlinear dynamics make it difficult to analytically assure stability of a dynamic gait – the robot state cannot be checked against closed-form balance conditions like (1). Walking trajectories from perturbed initial conditions are computed in simulation to verify stability [13].

The planar two-link "compass-gait" biped was shown to have passively stable hybrid limit cycles without any actuation whatsoever on shallow slopes [33]. Active control strategies have been designed to exploit passive dynamics for efficient planar walking on arbitrary slopes (e.g., [23], [38], [39], [44], [45]). For example, feedback linearization is used to zero output functions (i.e., virtual constraints) for some optimized gait based on hybrid zero dynamics [44], [45]. This was experimentally demonstrated on the planar bipeds RABBIT [44] and MABEL [40]. Feedback control has also enabled motion planning for planar dynamic walking, such as step-level planning over irregular terrain [32], [34]. A rigorous framework for controlling the planned flight trajectories in planar dynamic running was developed in [21].

There has only been scattered success in scaling these feedback control and planning methods into 3D space. The frontal plane-of-motion contributes instabilities resembling an inverted pendulum, and yaw dynamics in the transverse plane-of-motion must be controlled to variable headings with some sense of stability. Early attempts on spatially 3D walking constrained this complexity by fixing yaw motion [2], [7], [28]. The energy-shaping methods of controlled symmetries [39], passivity-based control [38], and controlled reduction [2], [20] exploit the geometric structure inherent in robot dynamics of arbitrary dimensionality. These strategies were used to decouple a fully 3D biped's sagittal plane-of-motion, which has well-known passive limit cycles, and from this build pseudo-passive walking gaits for the full-order system [17], [19], [20]. This simplified the search for full-order hybrid limit cycles and significantly expanded the class of 3D bipeds that can achieve pseudo-passive walking.

This framework was used to construct straight-ahead 3D walking gaits that can be steered toward nearby headings [17], [20]. Constant-curvature steering (fixed heading change between steps) was shown in [18], [19] to induce stable hybrid limit cycles modulo yaw, which serve as strategies for walking through 3D environments [15]. Straight-ahead gaits capable of steering along curves of mild curvature were also produced with hybrid zero dynamics [8], [35]. This approach elegantly exploits the fact that local asymptotic stability (LAS) implies local input-to-state stability: there exist bounds on path curvature and initial conditions that guarantee a bounded change in state between impacts. However, it is not clear how to derive the bounds for this form of stability (e.g., what is the maximum curvature safely allowed from some initial state).

We will instead estimate bounds on curvature and switching within a set of pre-stabilized LAS gaits. None of the aforementioned works on 3D dynamic walking combine control theory with planning applications, which we address in this paper.

C. Contribution of the Paper

In order to enable fast and efficient robot walkers in real-world environments, we present a planning framework for dynamic walking with high path curvature and guaranteed stability. The previously discussed planning techniques embrace two distinct control philosophies: the search for a desirable path and control inputs is integrated (feedback motion planning) in [32], [34], [41]; or the control system is designed to track a separately planned trajectory in [22], [26], [46]. We propose a third approach for the purpose of 3D dynamic walking: the planner is designed around the stability properties of a set of control systems serving as motion primitives. We are unaware of other planning results for dynamic walking in 3D space.

We define a class of hybrid dynamical systems that mathematically describe bipedal walking in Section II. We use this construction in Section III to formalize the notion of *asymptotically stable gait primitives* for a class of mechanical systems with impulses that admit an asymptotically stable hybrid limit cycle. We show in Section IV that a walking mechanism with a set of gait primitives can be formulated as a discrete-time switched system that sequentially composes gait primitives from step to step. We derive bounds on primitive curvature and switching frequency that stabilize this system, implying that a walking path composed of these primitives may be stably followed by the robot. This admits the common planning problem of exploring a discrete search tree with branching factor equal to the cardinality of the primitive set.

As an example of this framework, we derive a set of gait primitives for the 3D compass-gait biped using reduction-based control in Section V. These dynamic motion primitives are associated with constant-curvature walking arcs that grow a tree of possible paths in the workspace. We examine the growth of transient drift and implement a discrete search algorithm to demonstrate the accuracy of simulated walking along pre-planned paths (not previously addressed in [15]). We conclude with remarks and future work in Section VI.

II. Bipedal Walking as a Hybrid System

In order to study locomotion with impulsive impacts, we must consider both continuous and discrete dynamics in a hybrid system. Bipedal walking gaits correspond to hybrid limit cycles that are stable from step to step. For the example in this paper, we describe the hybrid dynamics of a particular class of bipedal walkers. We assume the discrete impact events are instantaneous and perfectly plastic. During the continuous single-support phase, the stance foot is assumed to remain in contact with the ground without slipping. However, these assumptions can be relaxed and still produce asymptotically stable walking [35], [37], [44] needed to apply the main result of this paper. We now define this class of hybrid systems to motivate our general formulation of gait primitives.

A. Continuous Single-Support Dynamics

We first derive the biped's continuous single-support dynamics using Lagrangian mechanics. Letting q denote a configuration in the robot's n-dimensional configuration space $\mathcal{Q}$, the system state is $x = (q^T, \dot{q}^T)^T$ in phase space $T\mathcal{Q}$ (all configurations and tangential velocities). As a notational reference, we arrange a general 3D biped's configuration vector into $q = (\psi, \varphi^T, \theta^T)^T$, where ψ is the scalar heading (yaw) variable, φ is the vector of frontal-plane (roll/lean) variables, and θ is the vector of sagittal-plane (pitch) variables. The world coordinates of the support foot remain constant during each cycle but will later be modeled for path planning.

The robot's kinetic and potential energies define the Lagrangian function, given in coordinates by

$$\mathcal{L}(q, \dot{q}) \;=\; \mathcal{K}(q, \dot{q}) - \mathcal{V}(q) \;=\; \frac{1}{2}\dot{q}^T M(q)\dot{q} - \mathcal{V}(q), \qquad (2)$$

where the kinetic energy is expressed in terms of the $n \times n$ inertia/mass matrix M. Integral curves on $T\mathcal{Q}$ necessarily satisfy the *Euler-Lagrange* (E-L) equations of this function:

$$\frac{d}{dt}\nabla_{\dot{q}}\mathcal{L} - \nabla_q \mathcal{L} \quad = \quad \tau. \qquad (3)$$

This yields the 2nd-order ordinary differential equations

$$M(q)\ddot{q} + C(q, \dot{q})\dot{q} + N(q) \quad = \quad Bu, \qquad (4)$$

where $n \times n$-matrix C contains the Coriolis/centrifugal terms, $N = \nabla_q \mathcal{V}$ is the vector of potential torques, and $n \times m$-matrix B maps the m-dimensional control input u to the n-dimensional joint torques τ ($m \leq n$). Control input u is subject to actuator saturation at torque constant $U^{\max}$.

We now incorporate the impulsive impact events associated with instantaneous double-support into a hybrid system.

B. Hybrid Dynamical Systems

We begin with some formalisms for hybrid systems from [2], [44]. Since knee-lock impacts introduce another level of complexity to the hybrid model, we only consider discrete events associated with foot-ground impacts (which does not preclude knees without impacts [44]). We therefore define hybrid models with one continuous phase, i.e., "systems with impulse effects." A *hybrid control system* has the form

$$\mathscr{HC} : \begin{cases} \dot{x} = f(x) + g(x)u & x \in D \backslash G \\ x^+ = \Delta(x^-) & x^- \in G \end{cases},$$

where $G \subset D$ is called the *guard* and $\Delta : G \to D$ is the *reset map*. We model walking on a flat surface by defining domain $D \subset T\mathcal{Q}$ as the set of states with nonnegative swing foot height. Guard G is then the set of states x for which this height is zero and decreasing, and the resulting impact event is modeled by discontinuous impact map Δ.

Given a controller for input u, we have a closed-loop hybrid system $\mathscr{H}$ solved by a curve $x(t)$ called a *hybrid flow*. An appropriately designed controller will produce walking gaits that typically repeat every two steps due to bilateral symmetry, so we must also define periodicity. A walking gait that repeats every h steps corresponds to an h-periodic hybrid flow $x(t)$, such that $x(t) = x(t + \sum_{i=1}^{h} T_i)$ for all $t \geq 0$, where T_i is the fixed *time-to-impact* between the $(i-1)^{th}$ and i^{th} discrete events. The image of such a hybrid flow in $T\mathcal{Q}$ is an invariant set called an h-periodic *hybrid orbit*

$$\mathcal{O} \quad = \quad \left\{ x \in D \mid x = x(t), t \in [0, \sum_{i=1}^{h} T_i] \right\}. \qquad (5)$$

If a periodic hybrid orbit is isolated, rather than one in a continuum of orbital solutions, it is called a *hybrid limit cycle*. We must now consider orbital stability of hybrid limit cycles in order to account for perturbations in bipedal locomotion.

III. Asymptotically Stable Gait Primitives

Although this definition of hybrid system only applies to a particular class of bipedal walkers, we can define gait primitives for any mechanical system that admits asymptotically stable hybrid limit cycles (discrete events can be trivially defined to consider smooth systems). We first offer the relevant forms of orbital stability in a general hybrid system.

A periodic hybrid orbit $\mathcal{O}$ is said to be (locally) asymptotically stable if all hybrid flows initiated in a neighborhood of $\mathcal{O}$ asymptotically approach the orbit. To be precise, we define a stronger sense of stability: a hybrid orbit $\mathcal{O}$ is (locally) *exponentially* stable (LES) if there exist constants $k, \alpha, \gamma > 0$ such that for all hybrid flows $x(t)$ with $d(x(t_0), \mathcal{O}) < \gamma$,

$$d(x(t), \mathcal{O}) \quad \leq \quad k e^{-\alpha(t-t_0)} d(x(t_0), \mathcal{O}) \qquad (6)$$

for all $t \geq t_0$. The distance function from vector x to set $\mathcal{O}$ in Euclidean metric space $(\mathbb{R}^{2n}, d)$ is $d(x, \mathcal{O}) := \inf_{y \in \mathcal{O}} ||x - y||$.

Orbital stability is determined using the method of *Poincaré sections* [44], which analyzes the *Poincaré return map* $P : G \to G$ associated with hybrid system $\mathscr{H}$. This is a discrete map defined on some hyperplane $G \subset T\mathcal{Q}$ (we choose the guard), which characterizes the evolution of hybrid flows between intersections with G. In particular, the h-composition of this map sends state $x_j \in G$ ahead h impact events by the discrete system $x_{j+h} = P^h(x_j)$. In the case of an h-periodic hybrid orbit $\mathcal{O}$, we have an *h-fixed point* $x^* \in G \cap \mathcal{O}$ such that $x^* = P^h(x^*)$. We then know that periodic hybrid orbit $\mathcal{O}$ is LES if and only if the associated fixed point x^* is LES in the discrete-time system defined by return map P.

We cannot analytically calculate this nonlinear map to determine its stability about x^*, but we can numerically approximate it through simulation [13]. This allows us to locally analyze orbital stability as a linear discrete system by the map's linearization, δP^h, where exponential stability is equivalent to the eigenvalue magnitudes of δP^h being strictly within the unit circle. The local stability region about h-fixed point x^*, known as the *basin of attraction*, is defined as

$$BoA(x^*) \quad = \quad \left\{ x \in G \;\; \text{s.t.} \lim_{z \to \infty} P^{hz}(x) = x^* \right\}. \qquad (7)$$

The numerical details of Poincaré analysis are deferred to [13].

We can now formalize asymptotically stable gait primitives corresponding to strategies for walking in 3D space.

Definition 1: An *asymptotically stable gait primitive* is a pair $\mathcal{G} = (P^h_{\text{cl}}, x^*)$, where closed-loop Poincaré map P_{cl} has the asymptotically stable h-fixed point x^* (modulo yaw).

Turning gaits are asymptotically stable about a fixed change in heading, $s = \bar{\psi} - \psi$. Straight-ahead gaits are asymptotically stable about a zero steering angle, i.e., a fixed heading $\psi = \bar{\psi}$. For the purpose of 3D dynamic walking on flat ground, we require that gait primitives can be arbitrarily oriented about the z-axis to walk from any initial heading.

Property 1: Given $\mathcal{G} = (P_s^h, x_\psi^*)$ with heading ψ and steering angle $s = \bar{\psi} - \psi$, where $\bar{\psi}$ is the h-step heading,

$$x_{\psi'}^* \quad := \quad x_\psi^* + (\rho \quad 0_{2n-1})^T$$

is an LES h-fixed point of P_s^h with heading $\psi' = \psi + \rho$ and steering angle $s = (\bar{\psi} + \rho) - \psi'$, for any $\rho \in \mathbb{S}^1$.

By construction, gait primitives are also independent of world position and time. This spatial-temporal symmetry allows primitives from a general set $\mathcal{P}^s = \{\mathcal{G}^{\mathrm{st}}, \mathcal{G}^{\mathrm{tu}(s)}, \mathcal{G}^{\mathrm{tu}(-s)}\}$, continuously parameterized by s, to be sequentially composed from step to step. Each gait has a nominal walking arc on the ground plane, with which walking paths are planned in $\mathrm{SE}(2)$.

IV. Planning with Gait Primitives

Given a set of asymptotically stable gait primitives, we can augment our hybrid model with an event-based (or stride-to-stride) control input yielding the discrete-time switched system

$$x(i+1) \quad = \quad P_{\sigma(i)}\left(x(i)\right), \tag{8}$$

where, at every impact event, switching signal $\sigma : \mathbb{Z}_+ \to \{0, s, -s\}$ chooses a closed-loop system $P_{\sigma(i)}$ associated with a gait primitive (parameterized by steering angle). Switching between closed-loop systems from the primitive set causes transients in system state, so we must derive rules for stability in the sequential composition of gait primitives.

A. Rules for Sequential Composition

We present a discrete switched system formulation of the funneling approach to composing controllers [4]. Let $\mathcal{P}^s$ be a discrete primitive set for a general biped, where we do not necessarily have a closed-form expression for the return map.

A biped employs gait primitive $\mathcal{G}^i = (P_i^h, x_i^*)$ during step cycle i by implementing the controller yielding Poincaré map P_i of closed-loop hybrid system $\mathscr{H}^i$. This is characterized by the system state and primitive choice (oriented coincident with the biped's heading) at every impact event.

Definition 2: Step cycle i is represented by the pair $\mathcal{T}_i = (x_{i-1}, \mathcal{G}^i)$, where $\mathcal{G}^i$ is the gait primitive employed after the $i-1^{th}$ impact event with impact state x_{i-1}. Moreover, $\mathcal{T}_i$ is said to be *switching* if $\mathcal{G}^i \neq \mathcal{G}^{i-1}$.

Step cycle $\mathcal{T}_{i+1}$ is then related to $\mathcal{T}_i$ by $x_i = P_i(x_{i-1})$. The biped may switch primitives at an impact before completing the h-step gait cycle of the current primitive (when $h > 1$).

Definition 3: A step cycle $\mathcal{T}_i = (x_{i-1}, \mathcal{G}^i)$ is *stable* if $x_{i-1} \in BoA(x_i^*)$, where x_i^* is the LES h-fixed point of return map P_i from gait primitive $\mathcal{G}^i$.

By invariance of the basin of attraction, if $\mathcal{T}_i$ is stable and $\mathcal{G}^{i+1} = \mathcal{G}^i$, then $\mathcal{T}_{i+1}$ is stable. We derive rules for switching stability by exploiting a convergence property of a bounded range of continuously parameterized gait primitives:

Assumption 1: For every steering angle $s \in [-S, S]$, there exists LES h-fixed point $x^{*\mathrm{tu}(s)}$ of $P_{\mathrm{tu}(s)}$ with corresponding $BoA(x^{*\mathrm{tu}(s)})$. Then, by definition there exists a non-empty open ball of radius $r_s > 0$ about $x^{*\mathrm{tu}(s)}$ such that

$$\mathcal{B}(x^{*\mathrm{tu}(s)}, r_s) \subset BoA(x^{*\mathrm{tu}(s)}),$$

where $x^{*\mathrm{tu}(s)}$ and r_s are assumed continuous functions of s.

Property 2: Turning h-fixed point $x^{*\mathrm{tu}(s)}$ converges to straight-ahead h-fixed point $x^{*\mathrm{st}} = x^{*\mathrm{tu}(0)}$ in metric space $(\mathbb{R}^{2n}, d)$ as $|s| \to 0$, where d is Euclidean distance. Formally speaking, $\lim_{|s|\to 0} r_s^* = 0$ for $r_s^* := d(x^{*\mathrm{tu}(s)}, x^{*\mathrm{st}})$.

Turning motion more closely resembles straight-ahead motion for smaller steering angles. We know that turning curvature $\kappa = \pm 1/R$ converges to straight-line curvature $\kappa = 0$ as turning radius $R \to \infty \Leftrightarrow |s| \to 0$. Property 2 then follows from Assumption 1 by continuity. We now can exploit overlap in neighboring basins of attraction:

Lemma 1: Given Property 2, there exists positive steering angle $\bar{S} \leq S$ such that for all $s \in [-\bar{S}, \bar{S}]$:

1) $x^{*\mathrm{st}} \in BoA(x^{*\mathrm{tu}(s)})$
2) $x^{*\mathrm{tu}(s)} \in BoA(x^{*\mathrm{st}})$
3) $x^{*\mathrm{tu}(-s)} \in BoA(x^{*\mathrm{tu}(s)})$

Proof: [1.1] We first define minimal ball radius $r := \min_{s\in[-S,S]}(r_s)$, positive by compactness of $[-S, S]$, so

$$\mathcal{B}(x^{*\mathrm{tu}(s)}, r) \subset \mathcal{B}(x^{*\mathrm{tu}(s)}, r_s) \subset BoA(x^{*\mathrm{tu}(s)}),$$

for all $s \in [-S, S]$. Now, since $r > 0$ and $\lim_{|s|\to 0} r_s^* = 0$, $\exists\ \bar{S} \leq S$ such that $r_s^* < r$ for all $s \in [-\bar{S}, \bar{S}]$. Then, $x^{*\mathrm{st}} \in \mathcal{B}(x^{*\mathrm{tu}(s)}, r)$ for all $s \in [-\bar{S}, \bar{S}]$, and the claim follows.

[1.2] First, by definition of LES, $\exists\ r_\infty > 0$ such that $\mathcal{B}(x^{*\mathrm{st}}, r_\infty) \subset BoA(x^{*\mathrm{st}})$. Then, again $\exists\ \bar{S}$ such that $r_s^* < r_\infty$ for all $s \in [-\bar{S}, \bar{S}]$. Hence, $x^{*\mathrm{tu}(s)} \in \mathcal{B}(x^{*\mathrm{st}}, r_\infty)$ for all $s \in [-\bar{S}, \bar{S}]$, and the claim follows.

[1.3] Recall $x^{*\mathrm{tu}(s)} \to x^{*\mathrm{st}}$ as $|s| \to 0$, which means that for each $\epsilon/2 > 0$, $\exists\ \delta > 0$ such that for all $s \in [-\delta, \delta]$, $d(x^{*\mathrm{tu}(s)}, x^{*\mathrm{st}}) < \epsilon/2$. Then, the triangle inequality shows

$$\begin{aligned} d(x^{*\mathrm{tu}(s)}, x^{*\mathrm{tu}(-s)}) \quad &\leq \quad d(x^{*\mathrm{tu}(s)}, x^{*\mathrm{st}}) + d(x^{*\mathrm{tu}(-s)}, x^{*\mathrm{st}}) \\ &< \quad \epsilon. \end{aligned}$$

Hence, if $r_s^{*\mathrm{tu}} := d(x^{*\mathrm{tu}(s)}, x^{*\mathrm{tu}(-s)})$, then $\lim_{s\to 0} r_s^{*\mathrm{tu}} = 0$.

Now, denoting each turning ball as $\mathcal{B}(x^{*\mathrm{tu}(s)}, r_s)$, we can define minimal ball radius $r := \min_{s\in[-S,S]}(r_s) > 0$. As we saw in 1.1, $\exists\ \bar{S}$ such that $r_s^{*\mathrm{tu}} < r$ for all $s \in [-\bar{S}, \bar{S}]$. Then, $x^{*\mathrm{tu}(-s)} \in \mathcal{B}(x^{*\mathrm{tu}(s)}, r)$ for all $s \in [-\bar{S}, \bar{S}]$, and the claim follows. Equivalently, $x^{*\mathrm{tu}(s)} \in BoA(x^{*\mathrm{tu}(-s)})$.

Finally, we can take the minimum of $\bar{S}$ from each proof to find $\bar{S}$ for the overall Lemma. ■

Remark 1: $\mathcal{B}(x^{*\mathrm{tu}(s)}, r)$ is an open ball so $x^{*\mathrm{st}}$ cannot be on the boundary of $BoA(x^{*\mathrm{tu}(s)})$. Therefore, points sufficiently close to $x^{*\mathrm{st}}$ are also contained in $BoA(x^{*\mathrm{tu}(s)})$. The same holds for the other three claims in Lemma 1.

Asymptotic stability implies convergence to fixed points in infinite time (exponentially fast in our case), but trajectories will eventually be close enough to stably switch gaits. Given enough time along a primitive, the biped's state will be funneled into the basin of attraction of the next desired primitive.

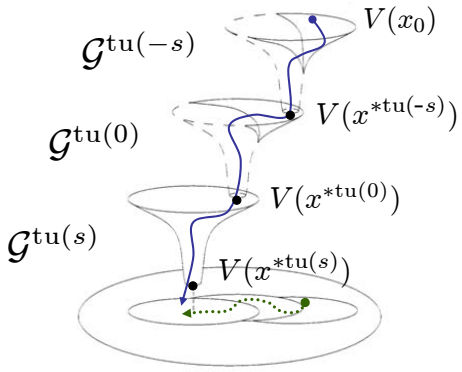

Fig. 1. Sequential composition of Lyapunov funnels, each being the graph of a Lyapunov function over its state space (illustrated as circular neighborhoods in a planar global space). The funneled state trajectory (dotted green) corresponds to the trajectory of the funneled Lyapunov functions (solid blue). Figure obtained and modified from [4].

This is called the *dwell time* of switching signal $\sigma(\cdot)$ in (8). This signal must be constrained to ensure stable composition of primitives, for which we invoke our main result:

Theorem 1: Given Property 2, then for any $s \in [-\bar{S}, \bar{S}]$ there exists a minimum number of steps $N \geq 1$, i.e., a lower bound on dwell time, such that for all integers $k \geq N$:

1) If $x \in BoA(x^{*\mathrm{st}})$, then $P^k_{\mathrm{st}}(x) \in BoA(x^{*\mathrm{tu}(s)})$.
2) If $x \in BoA(x^{*\mathrm{tu}(s)})$, then $P^k_{\mathrm{tu}(s)}(x) \in BoA(x^{*\mathrm{st}})$.
3) If $x \in BoA(x^{*\mathrm{tu}(s)})$, then $P^k_{\mathrm{tu}(s)}(x) \in BoA(x^{*\mathrm{tu}(-s)})$.

Proof: This follows directly from Lemma 1 and the definition of asymptotic convergence (cf. [1], [4] for analogous proofs concerning continuous-time switched systems). ■

Corollary 1: For any $s \in [-\bar{S}, \bar{S}]$, there exists a minimum dwell time $N \geq 1$ such that for any integer $k \geq N$, any switching step cycle $\mathcal{T}_{i+k}$ that follows a stable step cycle $\mathcal{T}_i$ is also stable.

Hence, a hierarchical controller (such as a finite-state machine) can easily constrain $\sigma(\cdot)$ for stable path planning, piecing together straight and curved gait segments such that the turns are not too sharp or the primitive switches too frequent. The steering sharpness must be bounded by steering angle $\bar{S}$, a condition that can be verified in simulation. However, minimum dwell time N depends explicitly on each gait primitive's basin of attraction and rate of exponential convergence, both of which can only be characterized numerically. We will examine this lower bound using exhaustive simulation in Section V-D.

B. Planning Formulation

Given these switching rules, we can define stable walking over a sequence of sequentially composed gait primitives.

Definition 4: A w-step *walking path execution* from initial condition $x(0) = x_0$ is defined by the ordered set $\mathcal{E}(x_0) = (\mathcal{T}_1, \mathcal{T}_2, \ldots, \mathcal{T}_w)$, where $\mathcal{T}_1 = (x_0, \mathcal{G}^1)$. A walking path execution $\mathcal{E}(x_0)$ is *robust* if all steps $\mathcal{T}_i$ are stable.

This corresponds to a trajectory of composed walking arcs on the ground surface $\mathbb{R}^2$. Recall that state x describes the robot's motion with respect to its joints. In the context of path planning on a level walking surface, we need to consider the robot's $\mathrm{SE}(2)$ coordinates with respect to a world frame, i.e., the Euclidean coordinates of (x, y)-position (e.g., measured at the stance foot) and heading ψ. Hence, every step i has an associated world configuration $c_i = (x^i_{\mathrm{pos}}, y^i_{\mathrm{pos}}, \psi_i)^T \in \mathrm{SE}(2)$. The extension of a biped's discrete state to $x^{\mathrm{e}}_i = (x^i_{\mathrm{pos}}, y^i_{\mathrm{pos}}, x^T_i)^T$ is trivial, as the new coordinates are easily updated by extended map P^{e}_i according to robot kinematics.

We denote a boundary-constrained w-step path execution as $\mathcal{E}^{c_w}_{c_0}(x^{\mathrm{e}}_0)$, where c_0 is from $x^{\mathrm{e}}_0 = (c^T_0, \varphi^T_0, \theta^T_0, \dot{q}^T_0)^T$ and c_w is from $x^{\mathrm{e}}_w = P^{\mathrm{e}}_w\left(x^{\mathrm{e}}_{w-1}\right) = (c^T_w, \varphi^T_w, \theta^T_w, \dot{q}^T_w)^T$. We can now invoke Theorem 1 to define paths for stable walking between world configurations c_0 and c_f. We say that a final configuration c_f is reachable if there exists a non-empty class of robust path executions $\left\{\mathcal{E}^{c_w}_{c_0} | c_w = c_f, w \geq 1\right\}$. The finite set of gait primitives is continuously parameterized by s to provide a (large) continuous reachable set.

We plan these paths using walking arcs in $\mathrm{SE}(2)$. Transient effects from gait switching (i.e., step cycle trajectories converge back and forth between attractive orbits) prevent a fixed mapping from steps to path arcs, but each path segment is closely approximated by a nominal constant-curvature arc.

Definition 5: The *nominal walking arc* of primitive $\mathcal{G}$ is the tuple $\left(\delta x^*_{\mathrm{pos}}, \delta y^*_{\mathrm{pos}}, \delta\psi^*\right) \in \mathrm{SE}(2)$ of the gait's x-y axis and yaw displacements, respectively, from initial heading $\psi = 0$.

For the gait primitives we consider, the heading change equals the primitive's steering angle, i.e., $s = \bar{\psi} - \psi = \delta\psi^*$. In order to sequentially compose walking arcs with different orientations, we rotate the nominal arc's x-y coordinate frame with a group action of $\mathrm{SO}(2)$ to coincide with the initial heading ψ_i of the following step cycle $\mathcal{T}_{i+1}$:

$$\begin{pmatrix} \delta x^{i+1}_{\mathrm{pos}} \\ \delta y^{i+1}_{\mathrm{pos}} \end{pmatrix} = \begin{pmatrix} \cos(\psi_i) & -\sin(\psi_i) \\ \sin(\psi_i) & \cos(\psi_i) \end{pmatrix} \begin{pmatrix} \delta x^{*i+1}_{\mathrm{pos}} \\ \delta y^{*i+1}_{\mathrm{pos}} \end{pmatrix}.$$

These nominal arcs grow a discrete tree in $\mathrm{SE}(2)$ with branching factor three. We have thus reduced a complicated kinodynamic motion planning problem in $\mathbb{R}^2 \times T\mathcal{Q}$ to a discrete search problem in $\mathrm{SE}(2)$, where the planning algorithm is designed to output a robust sequence $\mathcal{S}$ of steering angles parameterizing gait primitives. This corresponds to an open-loop event-based controller that produces a constrained switching signal $\sigma(\cdot)$ in the extended switched system

$$x^{\mathrm{e}}(i+1) \quad = \quad P^{\mathrm{e}}_{\sigma(i)}\left(x^{\mathrm{e}}(i)\right), \tag{9}$$

We examine transient drift from pre-planned paths in Sections V-E and V-F, but we first construct an example primitive set.

V. Application to the Compass-Gait Biped

This planning framework can be applied to any mechanical system that admits hybrid limit cycles satisfying Properties 1-2. Model complexity only challenges the low-level control design, so we demonstrate the high-level theory on a simple 3D compass-gait biped (see [8], [16], [19], [35] for more anthropomorphic models that admit asymptotically stable gaits).

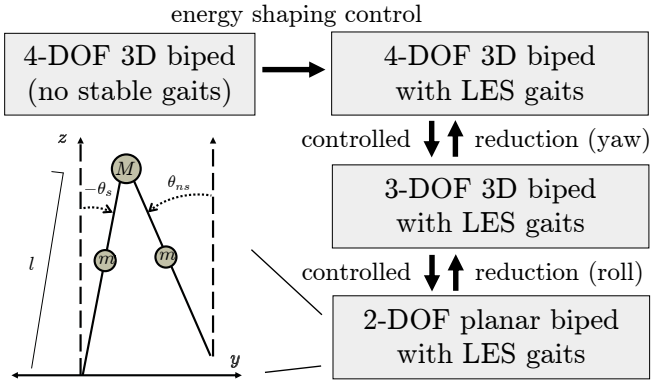

Fig. 2. Controlled reduction overview: the first reduction stage divides out the yaw DOF of the transverse plane, and the second stage divides out the lean DOF of the frontal plane, yielding the dynamics of the planar biped.

A. Modeling the Compass-Gait Biped

The 3D extension of the commonly studied planar compass-gait biped is shown in Fig. 2. This simple 4-DOF biped has no hip link, so each leg has identical single-support dynamics (walking gaits will be 1-step periodic). We now describe our biped's hybrid control system $\mathscr{HC}$.

We represent the configuration space of this biped by $\mathcal{Q} = \mathbb{T}^4$ with coordinate vector $q = (q_1^T, \theta^T)^T$, where the sagittal-plane and out-of-plane (scalar) variables are respectively contained in vectors $\theta = (\theta_{\rm s}, \theta_{\rm ns})^T$ and $q_1 = (\psi, \varphi)^T$. For simplicity we assume full actuation ($m = n$) including the point foot/ankle in stance, but recent control theoretic work considers phases of underactuation [37], yaw underactuation [14], or no actuation [35] at the stance ankle in 3D walking.

This robot's Lagrangian function $\mathcal{L}$ is defined by (2) in terms of 4×4 inertia/mass matrix

$$M(\varphi,\theta) \;=\; \left(\begin{array}{ccc} m_\psi(\varphi,\theta) & \multicolumn{2}{c}{\multirow{2}{*}{—}} & M_{\psi\varphi\theta}(\varphi,\theta) \\ | & & M_\varphi(\theta) & M_{\varphi\theta}(\theta) \\ M_{\psi\varphi\theta}^T(\varphi,\theta) & & M_{\varphi\theta}^T(\theta) & M_\theta(\theta) \end{array} \right),$$

where M_θ is the 2×2 inertia submatrix corresponding to the sagittal-plane DOFs. Note that M does not depend on ψ, so yaw is called a *cyclic* variable. We see that the lower-right 4×4 submatrix only depends on θ and thus has another cyclic variable φ. This *recursively cyclic* structure (a form of rotational symmetry) is shown to be a general property of open kinematic chains in [19], [20], which will be important to our control law design and satisfying Property 1.

The potential energy has a similar cyclic form $\mathcal{V}(\varphi,\theta) = \mathcal{V}_\theta(\theta)\cos(\varphi)$, containing the planar subsystem potential energy $\mathcal{V}_\theta$. These cyclic Lagrangian terms are used to derive the single-support dynamics (4), where torque map $B \in \mathbb{R}^{4\times4}$ is invertible for full actuation. Additional detail and expressions for these symbolic modeling terms are provided in [14].

We assign common physical parameters from the literature for our simulation results: M = 10 kg, m = 5 kg, l = 1 m, $U^{\max}$ = 20 Nm. We now describe a low-level controller to stabilize gaits for this biped, but recall that the planning framework does not depend on a specific motor control strategy.

B. Deriving a Stabilizing Low-Level Controller

Reduction-based control exploits the existence of cyclic variables to create controlled conservation laws that decompose robot dynamics into lower-dimensional control problems [14], [19], [20]. For our bipedal walker, we design momentum conservation laws that control yaw toward desired heading $\bar\psi$ in the transverse plane and stabilize lean about vertical $\bar\varphi = 0$ in the frontal plane (see Appendix). These conservation laws can be expressed as nonholonomic constraints, which are associated with an invariant surface in $T\mathcal{Q}$:

$$\mathcal{Z}_{\bar\psi} \;=\; \{(q,\dot q) \mid J_c(q)\dot q = b(q)\}, \tag{10}$$

where J_c and b are given in the Appendix. A geometric reduction with respect to these conservation laws defines a projection onto a reduced-order system corresponding to the decoupled sagittal plane-of-motion. Therefore, full-order LAS limit cycles can be constructed for locomotor patterns based on periodic motions in the sagittal plane.

The multistage controlled reduction of Fig. 2 is imposed by designing the control law such that the restriction of closed-loop system (4) to $\mathcal{Z}_{\bar\psi}$ is given by reduced-order planar system

$$M_\theta(\theta)\ddot\theta + C_\theta(\theta,\dot\theta)\dot\theta + N_\theta(\theta) \;=\; B_\theta v_\theta \tag{11}$$

associated with reduced Lagrangian

$$\mathcal{L}_\theta(\theta,\dot\theta) \;=\; \frac{1}{2}\dot\theta^T M_\theta(\theta)\dot\theta - \mathcal{V}_\theta(\theta). \tag{12}$$

Here, C_θ is the 2×2 Coriolis matrix derived from M_θ, $N_\theta = \nabla_q \mathcal{V}_\theta$, B_θ is the lower-right 2×2 submatrix of B, and $v_\theta \in \mathbb{R}^2$ is a subsystem control input yielding stable planar walking on flat ground (e.g., controlled symmetries [39]).

For this purpose, we would like to transform full-order Lagrangian $\mathcal{L}$ into a so-called *almost-cyclic* Lagrangian $\mathcal{L}_\lambda$, defined in coordinates as

$$\begin{aligned} \mathcal{L}_\lambda(q,\dot q) \;&:=\; \mathcal{L}(\varphi,\theta,\dot q) + \mathcal{L}_\lambda^{\rm aug}(q,\dot q) \\ &=\; \frac{1}{2}\dot q^T M_\lambda(\varphi,\theta)\dot q + Q_\lambda^T(q)\dot q - \mathcal{V}_\lambda(q), \end{aligned} \tag{13}$$

where the shaped inertia has two *Schur complements* of M:

$$M_\lambda \;=\; M - \left(\begin{array}{cc} 0 & 0 \\ 0 & \frac{-M_{\psi\varphi\theta}^T M_{\psi\varphi\theta}}{m_\psi} \end{array} \right) - \left(\begin{array}{cc} 0 & 0 \\ 0 & \frac{-M_{\varphi\theta}^T M_{\varphi\theta}}{m_\varphi} \end{array} \right)$$

and *gyroscopic* term Q_λ and potential energy $\mathcal{V}_\lambda$ depend on the cyclic variables through function $\lambda(q_1) = -K(q_1 - \bar q_1)$. We defer the detailed expressions for these terms to [14], [20].

Remark 2: An important property of $\mathcal{L}_\lambda$ is that the associated E-L equations render $\mathcal{Z}_{\bar\psi}$ invariant [14]. In order to account for initial conditions outside of $\mathcal{Z}_{\bar\psi}$, an auxiliary controller can be designed that further renders this surface globally attractive in D. This will also correct for constraint violations when changing the biped's desired heading, i.e., set-point $\bar\psi$ can be piecewise constant.

Proposition 1: The closed-loop Euler-Lagrange equations of $\mathcal{L}_\lambda$ restricted to $\mathcal{Z}_{\bar\psi}$ are given by planar system (11), i.e.,

$$\tfrac{d}{dt}\nabla_{\dot\theta}\mathcal{L}_\lambda - \nabla_\theta\mathcal{L}_\lambda\big|_{\mathcal{Z}_{\bar\psi}} = \tfrac{d}{dt}\nabla_{\dot\theta}\mathcal{L}_\theta - \nabla_\theta\mathcal{L}_\theta. \tag{14}$$

Proof: Note that $\mathcal{L}_\lambda^{\text{aug}}$ does not explicitly cancel any natural terms in $\mathcal{L}$. Therefore, shaped $\mathcal{L}_\lambda$ can be decomposed in terms of $\mathcal{L}_\theta$ and remainder terms grouped in function Rem:

$$\mathcal{L}_\lambda(q_1, \theta, \dot{q}_1, \dot{\theta}) \quad = \quad \mathcal{L}_\theta(\theta, \dot{\theta}) + \text{Rem}(q_1, \theta, \dot{q}_1, \dot{\theta}).$$

The shaping terms of $\mathcal{L}_\lambda$ are designed in [20] such that the E-L equations of Rem are zeroed on $\mathcal{Z}_{\bar{\psi}}$, implying restriction dynamics (14), equivalent to (11) of the planar biped. ■

Hence, geometric reduction of the shaped system projects onto decoupled planar system (11). Almost-cyclic form (13) is attained using Lagrangian-shaping torques that invert the dynamics then reinsert those dynamics plus augmenting terms:

$$\begin{aligned} u_\lambda(q, \dot{q}) &= B^{-1}\left(C(q, \dot{q})\dot{q} + N(q) + M(q)\left(\ddot{q}_{\text{des}} + v\right)\right) \\ \ddot{q}_{\text{des}} &:= M_\lambda^{-1}(q)\left(C_\lambda(q, \dot{q})\dot{q} + N_\lambda(q)\right), \end{aligned} \tag{15}$$

where matrix $C_\lambda(q, \dot{q}) = C_{M_\lambda}(q, \dot{q}) + C_{Q_\lambda}(q)$ contains the Coriolis terms from M_λ and the gyroscopic terms from Q_λ, vector $N_\lambda = \nabla_q \mathcal{V}_\lambda$ contains the potential torques, and v is some controller rendering $\mathcal{Z}_{\bar{\psi}}$ globally exponentially attractive (cf. [14]). We now use this to build a set of gait primitives.

C. Constructing the Primitive Set

Control law (15) yields closed-loop hybrid system $\mathscr{H}^{\text{st}}$ for straight-ahead walking on flat ground. For our example, we set $\bar{\psi} = 0$ without loss of generality and find the 1-fixed point $x^{*\text{st}}$ given in (16). We numerically verify LES of this straight-ahead gait by linearizing the associated Poincaré map P_{st}, and we denote the basin of attraction as $BoA_{\text{st}}(x^{*\text{st}})$. This defines the straight-ahead gait primitive $\mathcal{G}^{\text{st}} = (\mathscr{H}^{\text{st}}, x^{*\text{st}})$.

The associated hybrid orbit $\mathcal{O}^{\text{st}}$ is plotted in Fig. 3, showing its periodicity over one step. We see that this upright gait has no swaying in lean or yaw (which is to be expected for a hipless biped), and the sagittal plane has a periodic step length of 0.534 m and an approximate linear velocity of 0.727 m/s.

We create turning gaits by introducing a periodic disturbance into $\mathscr{H}^{\text{st}}$ in the form of constant steering between steps as in [15], [18]. We choose a steering angle s in the event-based controller to increment desired yaw $\bar{\psi}$ at each step (positively for CW or negatively for CCW). This yields closed-loop system $\mathscr{H}^{\text{tu}(s)}$. We want to show that for any sufficiently small $|s|$, this system's trajectories converge to a 1-step periodic orbit (modulo yaw) corresponding to a constant-curvature turning gait with an LES 1-fixed point:

$$x^{*\text{tu}(s)} + \begin{pmatrix} s & 0_{2n-1} \end{pmatrix}^T \quad = \quad P^{\text{tu}(s)}(x^{*\text{tu}(s)}) \tag{19}$$

with $BoA_{\text{tu}(s)}(x^{*\text{tu}(s)})$. We can then define CW-turning and CCW-turning gait primitives $\mathcal{G}^{\text{tu}(s)}$ and $\mathcal{G}^{\text{tu}(-s)}$, which have symmetric orbits with opposite yaw/lean.

Starting $\mathscr{H}^{\text{tu}(s)}$ from $x^{*\text{st}}$, we observe that hybrid flows converge to a 1-fixed point $x^{*\text{tu}(s)}$ associated with $\mathcal{O}^{\text{tu}(s)}$ for any choice of $s \in [-S, S]$, $S = 0.492$. We densely sample steering values in $[-S, S]$, finding the fixed point for each sample and confirming LES as numerical evidence of Assumption 1 and Property 2. For a sufficiently dense sampling, input-to-state stability guarantees that state trajectories will remain nearby for steering values s between samples (arguably resulting in unique LES fixed points).

The continuous evolution of the fixed point over this range of steering angles is shown in Fig. 4. We notice that increasing $|s|$ perturbs the sagittal-plane orbit compared to $\mathcal{O}^{\text{st}}$. The x- and y-axis displacements for the nominal walking arc associated with each steering angle (initialized from $\psi = 0$) are also given in Fig. 4. Increasing $|s|$ into the instability region outside $[-S, S]$, we observe period-doubling (flip) bifurcations yielding 2- and 4-step periodic LES orbits [14], ultimately leading to a chaotic strange attractor and falling.

We demonstrate a CW and CCW turning gait by choosing $\hat{s} = 0.32$, which corresponds to the fixed points in (17)-(18). The CW-turning gait is illustrated in the right-hand-side of Fig. 3 (and CCW by symmetry), which shows the gait's natural leaning into the turn. We see in Fig. 4 that the nominal walking arc for this CW gait primitive is characterized by $\delta x^*_{\text{pos}} = 0.1733$ m and $\delta y^*_{\text{pos}} = 0.5229$ m. The sign of δx^*_{pos} is flipped for the corresponding CCW gait. We verify that these turning motions do not violate unilateral ground contact constraints by calculating the ground reaction forces as in [14], [45].

These turning gaits naturally arise from our asymptotically stable straight-ahead system, without changing any reference trajectories. Integrating $\dot{q}^T\tau$ to obtain net work per step, the specific *mechanical cost of transport* for each gait is $c^{*\text{st}}_{\text{mt}} = 0.052$ and $c^{*\text{tu}(\pm\hat{s})}_{\text{mt}} = 0.058$, which compares favorably against the Cornell biped at $c_{\text{mt}} = 0.055$ and ASIMO at $c_{\text{mt}} = 1.6$ [10]. We now must numerically derive the stability bounds discussed in Section IV-A for this set of primitives.

D. Computing the Composition Rules

Although it is computationally difficult to find the exact region $[-\bar{S}, \bar{S}]$, we can easily verify containment for a particular s through simulation. We check convergence from all fixed points of primitive set $\mathcal{P}^{\hat{s}} = \{\mathcal{G}^{\text{st}}, \mathcal{G}^{\text{tu}(\hat{s})}, \mathcal{G}^{\text{tu}(-\hat{s})}\}$ to confirm the conditions of Lemma 1, i.e., $\hat{s} = 0.32 \in [\bar{S}, \bar{S}]$:

$$x^{*\text{st}}, x^{*\text{tu}(\hat{s})}, x^{*\text{tu}(-\hat{s})} \in BoA_{\text{st}} \bigcap BoA_{\text{tu}(\hat{s})} \bigcap BoA_{\text{tu}(-\hat{s})}.$$

This overlapping region also influences the minimum dwell time N for Theorem 1. If the biped's transient state leaves this overlapping safe region, an unstable switching scenario becomes possible. This is most likely caused by long primitive sequences with high frequency switching, which accumulate transient perturbations that cannot be attenuated during a short duration. Eventually, the impact-event state from one gait primitive may be outside the basin of attraction of the next.

We attempt to deduce N by exhaustively testing gait switching scenarios with a "random walk," picking a gait primitive every step from a uniform random distribution. We observe occasional falls after dozens of steps, implying that $N > 1$. We next allow switching every other step and are unable to produce falls after several lengthy simulations (400+ steps), suggesting that minimum dwell time $N = 2$. This is not a conservative estimate, but we have shown that falling scenarios are rarely encountered. Emerging work on transverse dynamics and sum-of-squares verification for basins of attraction of hybrid limit cycles [31], [42] may prove essential for conservative lower bounds on dwell time [1].

$$x^{*\mathrm{st}} \approx (0, 0, -0.2704, 0.2704, 0, 0, -1.4896, -1.7986)^T \quad (16)$$

$$x^{*\mathrm{tu}(\hat{s})} \approx (-0.0099, -0.0017, -0.2791, 0.2791, -0.0038, 0.0045, -1.5357, -1.9276)^T \quad (17)$$

$$x^{*\mathrm{tu}(-\hat{s})} \approx (0.0099, 0.0017, -0.2791, 0.2791, 0.0038, -0.0045, -1.5357, -1.9276)^T \quad (18)$$

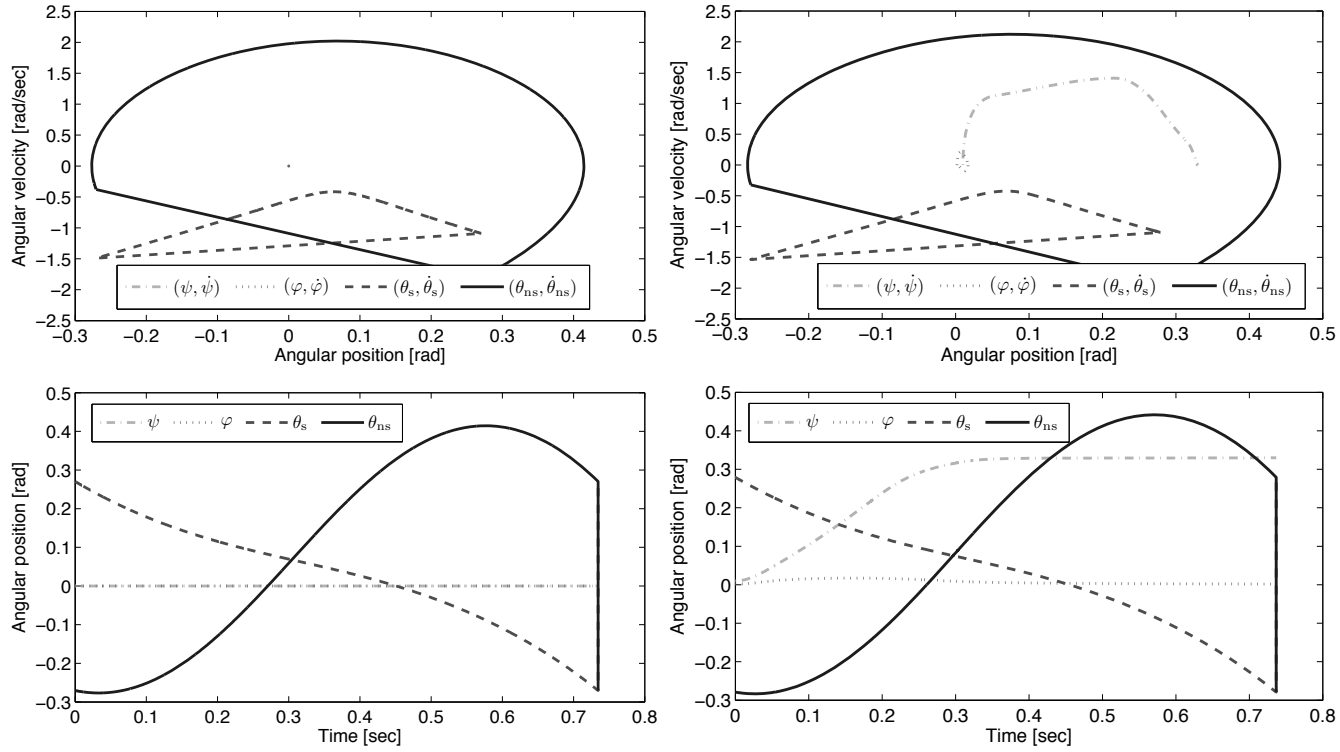

Fig. 3. Straight-ahead (left) and CW-turning (right) gaits: phase portrait (top) and coordinate trajectories (bottom).

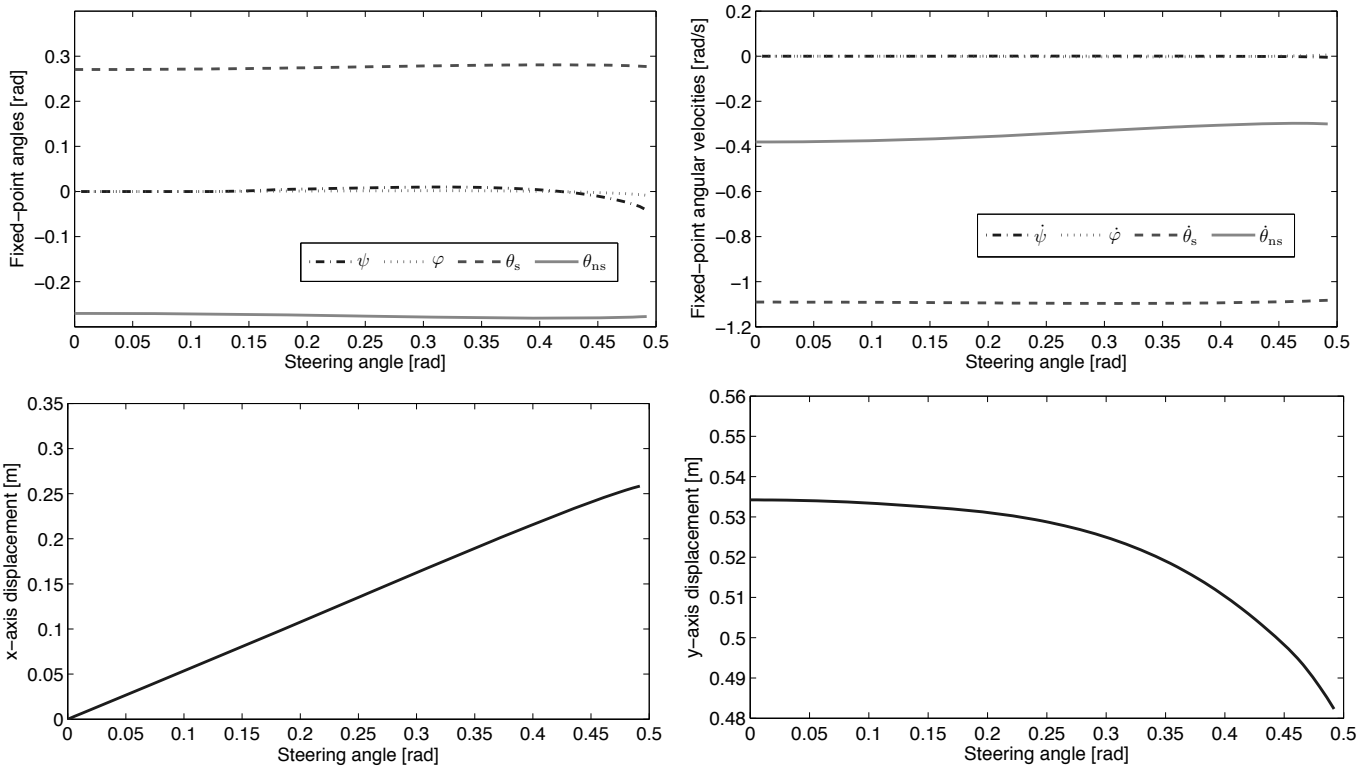

Fig. 4. Evolution of CW turning fixed point $x^{*\mathrm{tu}(|s|)}$ (top) and x-y axis displacements (bottom) over steering angle $s \in [0, 0.492]$.

TABLE I

Case	Steering Sequence			Simulated Drift (m)		
	Steps	Switches	Net Yaw	Max	Mean	Final
Random 1	72	36	0.32	0.540	0.226	0.538
Random 2	98	33	0.32	0.269	0.134	0.259
Planned 1	48	12	4.48	0.197	0.107	0.169
Planned 2	85	8	-0.32	0.168	0.105	0.168

These simulations provide evidence that the overlapping attractive region of the primitive set is large, due to the close proximity of the fixed points as well as the large sizes of the associated basins of attraction. Hence, this primitive set is capable of building a large class of robust walking paths, enabling path planning through 3D space (animated in Fig. 5).

E. Bounding Transient Drift

Before implementing a planning algorithm, we examine transient drift resulting from open-loop steering sequences in biped switched system (9). We generate 100 random steering sequences (step length between 10 and 100) from the primitive set $\mathcal{P}^{\hat{s}}$, computing the maximum, mean, and final drift values in Euclidean distance from the nominal walking path composed of primitive arcs. Trend lines are shown in Fig. 6.

All drift metrics tend to grow slowly linear with number of switches and even slower with number of steps, but net change in orientation alone has little influence on drift. Maximum drift is usually close or equal to final drift. Upon inspection of the extreme cases, we find that the direction of drift depends on the direction of switching (e.g., from straight-ahead to a single turning gait). Balancing the direction and timing of switches has a canceling effect on accumulated drift. We characterize two examples of this in Table I, where switching in random case 1 is heavily biased towards one turning gait resulting in more drift than case 2, which has more steps but balances switching between both turning gaits.

The maximum drift remains less than one step length in all but one of the 100 random cases. This suggests that the biped's actual trajectory stays bounded around any pre-planned path of bounded length (regardless of steering sequence). Drift accumulates slowly enough that plans need only be iteratively re-computed during very long walking paths (100+ steps). We can therefore define appropriately large obstacle safety regions and goal regions when planning open-loop paths through 3D environments. We now implement such a planning algorithm to provide open-loop control of switched system (9).

F. Planning Walking Paths

The gait primitive framework provides a layer of abstraction above the low-level control and stability of a walking mechanism to enable motion planning by switching between pre-stabilized gaits. We compose these separate gait primitives in discrete pieces, traditionally called motion primitives, to generate trajectories that simultaneously perform obstacle avoidance and direct the robot to a goal region in the workspace. In this section, we present one possible approach to planning based on gait primitives as a proof of concept of this hierarchical framework. It is important to recognize that the development of this paper gives us a parameterized set of motion primitives, which opens the possibility of a wide variety of planning algorithms being used in real robot systems.

For this demonstration, we choose the discrete set of motion primitives $\mathcal{P}^{\hat{s}}$, which corresponds to a discrete subset of the continuous range of steering angles available to the dynamic walker. Thus, the set of possible paths (concatenations of motion primitives) can be characterized by a tree data structure with branching factor equal to the cardinality b of the motion primitive set. The number of paths encoded in this tree expands exponentially as the number d of concatenated motion primitives in a path grows. Thus, the tree will represent $O(b^d)$ paths composed of nominal walking arcs. If d is large (the path length to be walked is long) and we wish to choose a path based on certain criteria, i.e., collision-free, reaches the goal, and minimizes a cost function, we will need to heuristically bias the exploration of the search tree. This is a well-studied problem [3], [9], [29], and in particular the A* Algorithm has been frequently applied to humanoid robots, e.g., [5], [27]. We will use a variant of [5] to plan our dynamic walking paths.

We define a goal region $R_{\mathrm{f}} \subset \mathrm{SE}(2)$ so that any robust walking path execution $\mathcal{E}_{c_0}^{c_w}(x_0^{\mathrm{e}})$ ending at world configuration $c_w \in R_{\mathrm{f}}$ is considered admissible. The planner outputs a steering sequence $\mathcal{S} \in \{s, 0, -s\}^w$ corresponding to the sequence of gait primitives for each step in walking execution $\mathcal{E}_{c_0}^{c_w}(x_0^{\mathrm{e}})$. This sequence is designed to produce a trajectory in system (9) that is collision free and terminates in the goal region while minimizing a scalarized objective function that penalizes nominal path length and number of gait switches:

$$\mathcal{C}\left[\mathcal{E}_{c_0}^{c_w}\right] = \sum_{i=1}^{w} \mathrm{norm}(\delta x_{\mathrm{pos}}^{*i}, \delta y_{\mathrm{pos}}^{*i}) + \alpha \mathbb{1}\{\mathcal{G}^{i-1} \neq \mathcal{G}^{i}\}, \quad (20)$$

where $\alpha = 0.7$, favoring shorter and smoother walking paths.

The planner begins by performing a workspace decomposition that bounds obstacles with safety regions and decomposes the free space into a set of convex cells. We use the shortest path on the workspace skeleton[1] to identify the path homotopy class[2] we will explore to find our path composed of motion primitives. This heuristic works well in practice for reducing the number of paths to be explored without removing desirable paths [5]. Our second complexity-reducing approximation is a branch and bound style of tree search, where we plan optimal sequences of motion primitives between subgoal regions in the configuration space. We identify these subgoals by finding intersections between workspace curves corresponding to the projection of paths belonging to our selected homotopy class and boundaries of the workspace decomposition.

We employ the A* Algorithm to compute optimal paths between subgoals. This algorithm expands the search tree by choosing nodes from a priority queue that is sorted by the *cost-to-come*, a partial computation of (20) on the segment of the primitive sequence explored thus far, plus the estimated *cost-to-go*. The true cost-to-go from a node, i.e., the minimal cost to reach the goal set from the configuration of that node, is

[1]The workspace skeleton is a deformation retract of the free workspace, implemented as a discrete approximation of the generalized Voronoi diagram.

[2]Two paths that are homotopic to one another are identical after a homotopic transformation corresponding to a deformation retract [9].

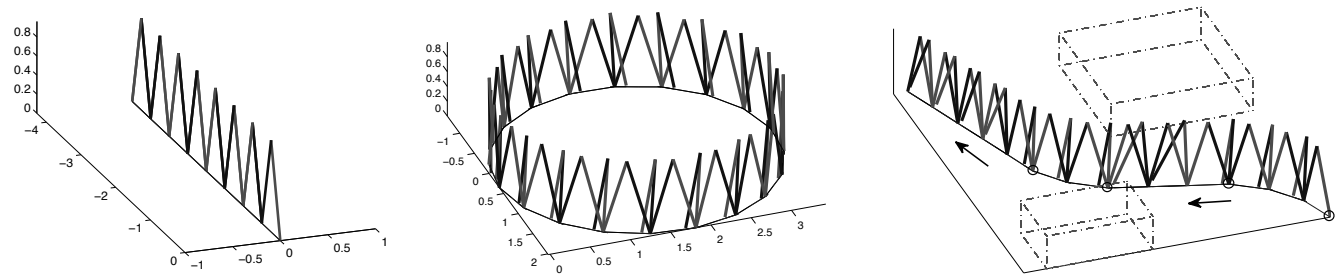

Fig. 5. Animations of S/CW gait primitives (left/middle) and an example planned walking execution (right). The sequence of primitives is (CCW, CCW, CCW, S, S, S, CW, CW, S, S, S, S, S), where switching steps are indicated by circles at impact events.

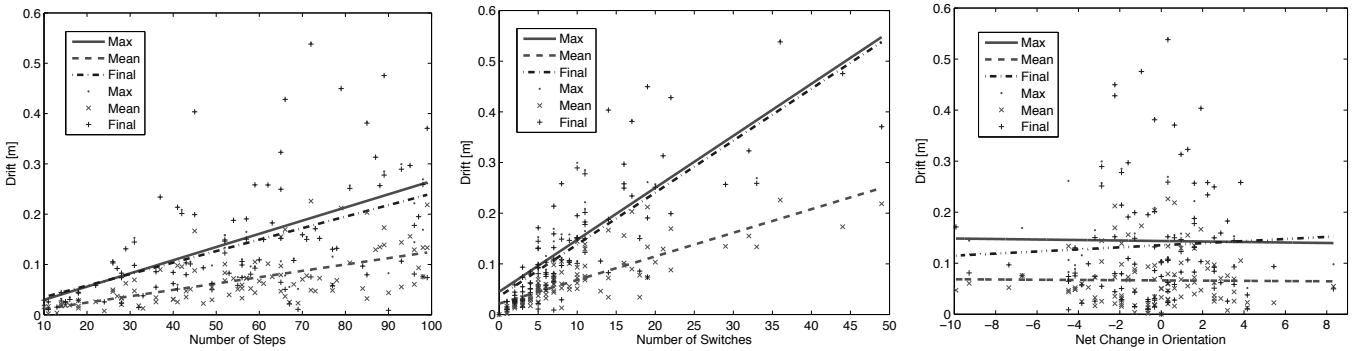

Fig. 6. Simulated maximum, mean, and final drift values (and regression lines) for 100 randomly generated steering sequences, against number of steps (left), number of switches (middle), and net change in orientation (right).

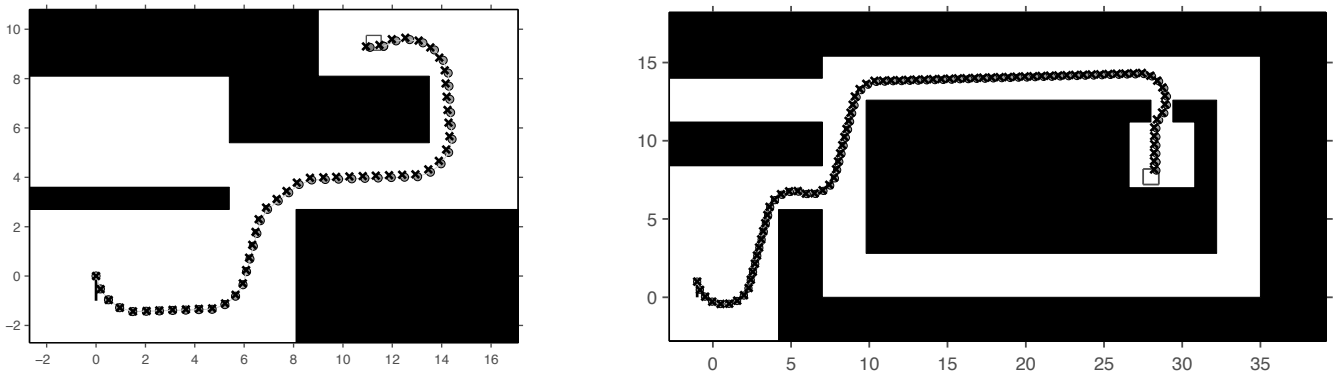

Fig. 7. Two planned walking environments with primitive set $\mathcal{P}^{\hat{s}}$, $\hat{s} = 0.32$. Planned steps are indicated by gray circles and simulated steps by black X's. Initial orientation is shown by a black line from the starting position. Supplementary downloadable videos available for planned walking cases.

not known until the algorithm completes, so it is approximated with a heuristic function that lower bounds the true cost-to-go. For this, we use the Euclidean distance between workspace projections of the robot's configuration at the node and the closest point in the current subgoal region. Sequences of motion primitives that violate dwell time constraints or likely cause obstacle collisions are pruned during the process of node expansion. When A* terminates, we are left with a path plan from one subgoal region to the next. We can then start a new search from the terminal configuration of this path to the next subgoal region. The final subgoal region is identical to the goal region, by which the plan generation is completed.

Given the example environments of Fig. 7, the planner takes seconds to produce the nominal paths shown in gray. The 4-DOF biped is then simulated with the corresponding sequence of gait primitives, resulting in a walking execution (shown in black) that traces the pre-planned path into the goal region with only minor drift. In both cases, the average and final errors from planned step placements, given in the bottom rows of Table I, are respectively 20% and 32% of one step length.

Recall that the biped does not explicitly track this planned path – rather, the nominal walking arcs associated with the open-loop primitive sequence accurately predict the walking path execution. This is noteworthy given the transient effects after each switching step. The observed drift may indeed accumulate over long paths, but occasional re-planning can compensate for this. We can also encode switching rules into a regular language [12] and use a finite-state machine (i.e., discrete automaton) for closed-loop path tracking.

VI. Conclusions

We reduced a complicated feedback motion planning problem in a high-dimensional state space to a much simpler discrete path planning problem with a lower-dimensional characterization of the robot's configuration. This allows decomposed, accurate planning of efficient bipedal locomotion based on human-like passive walking principles, which is fundamentally different from ZMP methods [22], [27], [46].

The planning framework of dynamic gait primitives can be used with any control method that produces asymptotically stable gaits (e.g., walking [8], [16], [19], [35], climbing [11], or running [36], [44]). Each gait primitive is characterized by its hybrid system and stable fixed point, thus corresponding to a nominal periodic hybrid orbit. In our compass-gait example, these orbits are naturally attractive by the (pseudo-passive) robot dynamics after controlled reduction. This motion is not prescribed by full-state trajectories [12] or subjected to postural constraint (1), yet we have robustness over a large class of paths composed of gait primitives.

In order to reach specific goal configurations, future work might generalize this framework to allow primitive switching within the full continuous range of available steering angles. Gait primitives and their stability rules might also be precomputed using the feedback motion planning method of randomized LQR trees [41] with sum-of-squares programming [31], [42]. Practical implementations of the gait primitive framework could integrate a suite of other feedback motion planning tools, such as step-level planning over rough terrain [32], [34] and time-scaling for variable walking speeds [23].

Experimental dynamic walking has been demonstrated on planar robots using hybrid zero dynamics (cf. [40], [44]), and 3D results may soon be possible with advances in actuator and biped mechanical design. Controlled reduction requires actuation at the stance ankle, but the yaw DOF input can be realized mechanically with a passive damper as shown in [14]. This would allow a more feasible (and arguably anthropomorphic) implementation with a 2-DOF ankle actuator for lean and pitch. In fact, the preliminary investigation of [16] aims to implement controlled reduction on the highly-redundant Sarcos humanoid robot [6], encouraging a future generation of fast and efficient humanoid walkers. Growing evidence for switching in human locomotor control (cf. [14, Chapter 7]) also motivates investigation into the existence of primitives in human motion planning.

Appendix: Controlling Cyclic Variables

We exploit the recursively cyclic structure of M by defining the generalized momentum $p = \hat{M}\dot{q}$ with respect to inertia matrix $\hat{M}$, defined by upper-triangular blocks from M:

$$\hat{M}(\varphi,\theta) = \begin{pmatrix} \hat{M}_1(\varphi,\theta) & M_{12}(\varphi,\theta) \\ 0 & M_2(\theta) \end{pmatrix},$$

where $M_2 = M_\theta$, and upper-triangular submatrix $\hat{M}_1 \in \mathbb{R}^{2\times 2}$ and off-diagonal matrix $M_{12} \in \mathbb{R}^{2\times 2}$ are given by

$$\begin{aligned} \hat{M}_1(\varphi,\theta) &= \begin{pmatrix} m_\psi(\varphi,\theta) & m_{\psi\varphi}(\varphi,\theta) \\ 0 & m_\varphi(\theta) \end{pmatrix} \\ M_{12}(\varphi,\theta) &= \begin{pmatrix} M_{\psi\theta}(\varphi,\theta) \\ M_{\varphi\theta}(\theta) \end{pmatrix}. \end{aligned}$$

Given "divided" coordinate vector $q_1 = (\psi,\varphi)^T$ and corresponding momenta p_1, we wish to enforce a *functional conservation law* that will stabilize q_1 and p_1:

$$\begin{aligned} p_1 &:= \begin{bmatrix} I_{2\times 2} & 0_{2\times 2} \end{bmatrix} \hat{M}\dot{q} = -K(q_1 - \bar{q}_1) \\ &\Leftrightarrow \begin{bmatrix} \hat{M}_1 & M_{12} \end{bmatrix} \dot{q} = -K(q_1 - \bar{q}_1) \\ &\Leftrightarrow \dot{q}_1 = -\hat{M}_1^{-1}\left[K(q_1 - \bar{q}_1) + M_{12}\dot{\theta}\right], \end{aligned} \qquad (21)$$

where $K \in \mathbb{R}^{2\times 2}$ is a diagonal positive-definite matrix of constant gains, and $\bar{q}_1 \in \mathbb{T}^2$ is a constant vector of desired set-points for coordinates q_1. I.e., we wish to render invariant the surface (10) in $T\mathcal{Q}$ associated with nonholonomic constraints, where $J_c = [\hat{M}_1 \quad M_{12}]$ and $b = -K(q_1 - \bar{q}_1)$ is continuously parameterized by desired set-point $\bar{q}_1$.

Due to the recursively cyclic and upper-triangular structure of $\hat{M}$, it is easily shown that scaling terms $\hat{M}_1^{-1}K$ and $\hat{M}_1^{-1}M_{12}$ in (21) have no dependence on ψ in the top row and additionally no dependence on φ in the bottom row. We then see that equation (21) represents a homogeneous first-order linear system in q_1 with time-varying coefficients based on the trajectories $(\theta(t), \dot{\theta}(t))$. Moreover, $\hat{M}_1^{-1}K$ is positive-definite by the positive-definiteness of inertia matrix M and consequently its diagonal blocks. Homogenous system (21) then has negative gain linearity in q_1, implying asymptotic stability given asymptotic stability in the reduced subsystem about some periodic solution $(\theta^*(t), \dot{\theta}^*(t))$ (cf. [14]).

In order to produce periodic trajectories in reduced coordinates $(\theta, \dot{\theta})$, which are naturally coupled to the divided coordinates, control law (15) is designed to both enforce (21) and render the sagittal plane-of-motion decoupled [16], [20].

References

[1] T. Alpcan and T. Basar, "A stability result for switched systems with multiple equilibria," *Dynamics of Continuous, Discrete and Impulsive Systems*, 2010, to appear.

[2] A. D. Ames, R. D. Gregg, and M. W. Spong, "A geometric approach to three-dimensional hipped bipedal robotic walking," in *IEEE Conf. Decision and Control*, New Orleans, LA, 2007, pp. 5123–5130.

[3] J. Barraquand and J.-C. Latombe, "Nonholonomic multibody mobile robots: Controllability and motion planning in the presence of obstacles," *Algorithmica*, vol. 10, no. 2, pp. 121–155, 1993.

[4] R. Burridge, A. Rizzi, and D. Koditschek, "Sequential composition of dynamically dexterous robot behaviors," *Int. J. Robotics Research*, vol. 18, no. 6, pp. 534–555, 1999.

[5] S. Candido, Y. T. Kim, and S. Hutchinson, "An improved hierarchical motion planner for humanoid robots," in *IEEE Int. Conf. Humanoid Robots*, Daejeon, Korea, 2008, pp. 654–661.

[6] G. Cheng, S.-H. Hyon, A. Ude, J. Morimoto, J. Hale, J. Hart, J. Nakanishi, D. Bentivegna, J. Hodgins, C. Atkeson, M. Mistry, S. Schaal, and M. Kawato, "CB: Exploring neuroscience with a humanoid research platform," in *IEEE Int. Conf. Robotics and Automation*, Pasadena, CA, 2008, pp. 1772–1773.

[7] C. Chevallereau, J. W. Grizzle, and C. Shih, "Asymptotically stable walking of a five-link underactuated 3D bipedal robot," *IEEE Trans. Robotics*, vol. 25, no. 1, pp. 37–50, 2008.

[8] C. Chevallereau, J. W. Grizzle, and C. L. Shih, "Steering of a 3D bipedal robot with an underactuated ankle."

[9] H. M. Choset, K. M. Lynch, S. Hutchinson, G. Kantor, W. Burgard, L. E. Kavraki, and S. Thrun, *Principles of Robot Motion*. Cambridge, MA: MIT Press, 2005.

[10] S. H. Collins and A. Ruina, "A bipedal walking robot with efficient and human-like gait," in *IEEE Int. Conf. Robotics and Automation*, Barcelona, Spain, 2005, pp. 1983–1988.

[11] A. Degani, H. Choset, and M. T. Mason, "DSAC – dynamic, single actuated climber: Local stability and bifurcations," in *IEEE Int. Conf. Robotics and Automation*, Anchorage, AK, 2010, pp. 2803–2809.

[12] E. Frazzoli, M. A. Dahleh, and E. Feron, "Maneuver-based motion planning for nonlinear systems with symmetries," *IEEE Trans. Robotics*, vol. 21, no. 6, pp. 1077–1091, 2005.

[13] A. Goswami, B. Thuilot, and B. Espiau, "Compass-like biped robot part I: Stability and bifurcation of passive gaits," Institut National de Recherche en Informatique et en Automatique (INRIA), Grenoble, France, Tech. Rep. 2996, 1996.

[14] R. D. Gregg, "Geometric control and motion planning for three-dimensional bipedal locomotion," Ph.D. dissertation, University of Illinois at Urbana-Champaign, 2010.

[15] R. D. Gregg, T. W. Bretl, and M. W. Spong, "Asymptotically stable gait primitives for planning dynamic bipedal locomotion in three dimensions," in *IEEE Int. Conf. Robotics and Automation*, Anchorage, AK, 2010, pp. 1695–1702.

[16] R. D. Gregg, L. Righetti, J. Buchli, and S. Schaal, "Constrained accelerations for controlled geometric reduction: Sagittal-plane decoupling in bipedal locomotion," in *IEEE Int. Conf. Humanoid Robots*, Nashville, TN, 2010.

[17] R. D. Gregg and M. W. Spong, "Reduction-based control with application to three-dimensional bipedal walking robots," in *American Control Conf.*, Seattle, WA, 2008, pp. 880–887.

[18] ——, "Bringing the compass-gait bipedal walker to three dimensions," in *IEEE Int. Conf. Intelligent Robots and Systems*, St. Louis, MO, 2009, pp. 4469–4474.

[19] ——, "Reduction-based control of branched chains: Application to three-dimensional bipedal torso robots," in *IEEE Conf. Decision and Control*, Shanghai, China, 2009, pp. 8166–8173.

[20] ——, "Reduction-based control of three-dimensional bipedal walking robots," *Int. J. Robotics Research*, vol. 26, no. 6, pp. 680–702, 2010.

[21] J. W. Grizzle, C. H. Moog, and C. Chevallereau, "Nonlinear control of mechanical systems with an unactuated cyclic variable," *IEEE Trans. Automatic Control*, vol. 50, no. 5, pp. 559–576, 2005.

[22] K. Hauser, T. Bretl, J.-C. Latombe, K. Harada, and B. Wilcox, "Motion planning for legged robots on varied terrain," *Int. J. Robotics Research*, vol. 27, no. 11-12, pp. 1325–1349, 2008.

[23] J. K. Holm, D. Lee, and M. W. Spong, "Time-scaling trajectories of passive-dynamic bipedal robots," in *IEEE Int. Conf. Robotics and Automation*, Roma, Italy, 2007, pp. 3603–3608.

[24] Honda Worldwide, "Asimo walking technology," 2009. [Online]. Available: http://world.honda.com/ASIMO/technology/walking.html.

[25] K. Kaneko, F. Kanehiro, S. Kajita, H. Hirukawa, T. Kawasaki, M. Hirata, K. Akachi, and T. Isozumi, "Humanoid robot HRP-2," in *IEEE Int. Conf. Robotics and Automation*, New Orleans, LA, 2004, pp. 1083–1090.

[26] J. J. Kuffner Jr., S. Kagami, K. Nishiwaki, M. Inaba, and H. Inoue, "Dynamically-stable motion planning for humanoid robots," *Autonomous Robots*, vol. 1, no. 12, pp. 105–118, 2002.

[27] J. J. Kuffner Jr., K. Nishiwaki, S. Kagami, M. Inaba, and H. Inoue, "Motion planning for humanoid robots," in *Robotics Research*. New York, NY: Springer, 2005, pp. 365–374.

[28] A. D. Kuo, "Choosing your steps carefully: Walking and running robots," *IEEE Robotics and Automation Mag.*, vol. 14, no. 2, pp. 18–29, 2007.

[29] S. M. LaValle, *Planning Algorithms*. New York, NY: Cambridge University Press, 2006.

[30] W. R. Leonard and M. L. Robertson, "Energetic efficiency of human bipedality," *American J. Physical Anthropology*, vol. 97, pp. 335–338, 1995.

[31] I. R. Manchester, "Tranverse dynamics and regions of stability for nonlinear hybrid limit cycles," in *IFAC World Congress*, Milano, Italy, 2011, submitted for publication.

[32] I. R. Manchester, U. Mettin, F. Iida, and R. Tedrake, "Stable dynamic walking over rough terrain: Theory and experiment," in *14th Int. Symposium on Robotics Research*, Lucerne, Switzerland, 2009.

[33] T. McGeer, "Passive dynamic walking," *Int. J. Robotics Research*, vol. 9, no. 2, pp. 62–82, 1990.

[34] S. Ramamoorthy and B. Kuipers, "Trajectory generation for dynamic bipedal walking through qualitative model based manifold learning," in *IEEE Int. Conf. Robotics and Automation*, Pasadena, CA, 2008, pp. 359–366.

[35] C. Shih, J. W. Grizzle, and C. Chevallereau, "From stable walking to steering of a 3D bipedal robot with passive point feet," *Robotica*, 2010, submitted for publication.

[36] J. Shill, B. Miller, J. Schmitt, and J. E. Clark, "Design of a dynamically stable horizontal plane runner," in *IEEE Int. Conf. Robotics and Automation*, Anchorage, AK, 2010, pp. 4749–4754.

[37] R. Sinnet and A. D. Ames, "3D bipedal walking with knees and feet: A hybrid geometric approach," in *IEEE Conf. Decision and Control*, Shanghai, China, 2009, pp. 3208–3213.

[38] M. W. Spong, "The passivity paradigm in bipedal locomotion," in *Int. Conf. Climbing and Walking Robots*, Madrid, Spain, 2004.

[39] M. W. Spong and F. Bullo, "Controlled symmetries and passive walking," *IEEE Trans. Automatic Control*, vol. 50, no. 7, pp. 1025–1031, 2005.

[40] K. Sreenath, H. W. Park, I. Poulakakis, and J. W. Grizzle, "A compliant hybrid zero dynamics controller for stable, efficient and fast bipedal walking on MABEL," *Int. J. Robotics Research*, 2010, OnlineFirst.

[41] R. Tedrake, I. R. Manchester, M. M. Tobenkin, and J. W. Roberts, "LQR-Trees: Feedback motion planning via sums-of-squares verification," *Int. J. Robotics Research*, vol. 29, no. 8, pp. 1038–1052, 2010.

[42] U. Topcu, A. Packard, and P. Seiler, "Local stability analysis using simulations and sum-of-squares programming," *Automatica*, vol. 44, no. 10, pp. 2669–2675, 2008.

[43] M. Vukobratovic and B. Borovac, "Zero-moment point - thirty years of its life," *Int. J. on Humanoid Robotics*, vol. 1, no. 1, pp. 157–174, 2004.

[44] E. R. Westervelt, J. W. Grizzle, C. Chevallereau, J. H. Choi, and B. Morris, *Feedback Control of Dynamic Bipedal Robot Locomotion*. New York, NY: CRC Press, 2007.

[45] E. R. Westervelt, J. W. Grizzle, and D. E. Koditschek, "Hybrid zero dynamics of planar biped walkers," *IEEE Trans. Automatic Control*, vol. 48, no. 1, pp. 42–56, 2003.

[46] E. Yoshida, C. Esteves, I. Belousov, J.-P. Laumond, T. Sakaguchi, and K. Yokoi, "Planning 3-D collision-free dynamic robotic motion through iterative reshaping," *IEEE Trans. Robotics*, vol. 24, no. 5, pp. 1186–1198, 2008.